ACS OMEGA

http://pubs.acs.org/journal/acsodf

Article

Control and Preparation of Quaternized Chitosan and Carboxymethyl Chitosan Nanoscale Polyelectrolyte Complexes Based on Reactive Flash Nanoprecipitation

Rizwan Ahmed,[¶] Noor ul ain Hira,[¶] Zhinan Fu, Mingwei Wang,* Adeel Halepoto, Santosh Khanal, Shahid Iqbal, Hidayatullah Mahar, Martien Abraham Cohen Stuart, and Xuhong Guo*

Cite This: *ACS Omega* 2021, 6, 24526−24534

Read Online

ACCESS | Metrics & More | Article Recommendations | Supporting Information

ABSTRACT: Nanoscale polyelectrolyte complex materials have been extensively investigated for their promising application in protocell, drug carriers, imaging, and catalysis. However, the conventional preparation approach involving positive and negative polyelectrolytes leads to large size, wide size distribution, instability, and aggregation due to the nonhomogeneous mixing process. Herein, we employ reactive flash nanoprecipitation (RFNP) to control the mixing and preparation of the nanoscale polyelectrolyte complex. With RFNP, homogeneous mixing complexation between oppositely charged chitosan derivatives could be achieved, resulting in stable nanoscale complexes (NCs) with controllable size and narrow size distribution. The smallest size of NCs is found at specific pH due to the maximum attraction of positive and negative molecules of chitosan. The size can be modulated by altering the volumetric flow rates of inlet streams, concentration, and charge molar ratio of two oppositely charged chitosan derivatives. The charge molar ratio is also tuned to create NCs with positive and negative shells. There is no significant variation in the size of NCs produced at different intervals of time. This method allows continuous and tunable NC production and could have the potential for fast, practical translation.

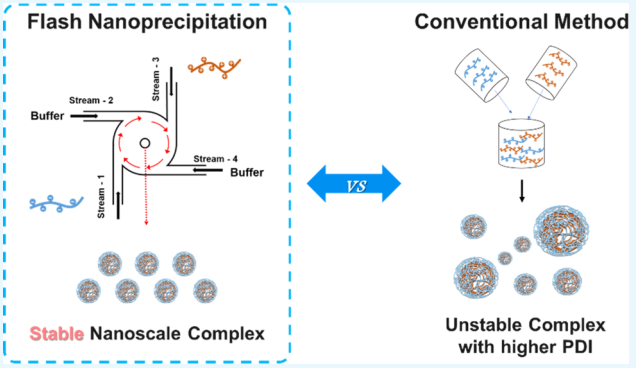

1. INTRODUCTION

Many attempts have been made to develop new delivery systems for bioactive compounds. As a drug nanocarrier, nanoparticles (NPs) have been widely used in delivery systems and show great potential in biomedical applications. FDA (Food and Drug Administration)-approved NPs are currently being used to treat metastatic pancreatic adenocarcinoma and ovarian cancer that has progressed or recurred after chemotherapy and as a contrast agent for magnetic resonance imaging of the liver.[1−4] Among many NP preparation methods including self-assembly or ionic crosslinking, polyelectrolyte complexation has recently attracted much attention, as it could form soft nanoscale materials rather than hard particles. Cationic and anionic water-soluble charged polyelectrolytes interact in an aqueous solution to form polyelectrolyte complexes.[5−8] It is a charge-driven process; the nanoscale complex (NC) sizes can be controlled by many factors such as the charge mixing ratio, nature of the chemical groups, and ionic strength. The preparation of the NC is typically achieved through manual mixing, vortexing, or dropwise addition under stirring. However, the stability of the formed NCs and the reproducibility of these methods are lacking. At the same time, the quality of NCs is often suboptimal, typically showing a broad size distribution and a high degree of variability due to nonhomogeneous mixing. Therefore, one of the significant challenges needed to be addressed is the controlled preparation of NCs.[9−12]

Different from many manual mixing methods, flash nanoprecipitation (FNP), invented by Johnson and Prud'homme in 2003, could offer a rapid and efficient homogeneous mixing for the facile controlled preparation of NPs,[13−15] and FNP is further developed by Zhu et al.[16−20] In FNP, amphiphilic diblock polymers (stabilizers) and hydrophobic active materials are dissolved in an organic phase and rapidly mixed with an antisolvent stream to produce controlled precipitation with tunable particle sizes (50−500 nm) and limited size distribution, in which supersaturation can be generated much faster than the diffusion-limited aggregation that controls NP

Received: June 7, 2021
Published: September 16, 2021

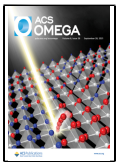

Scheme 1. Structure of QCS (a) and CMCH (b). (c) Illustration of the Preparation of NCs by RFNP

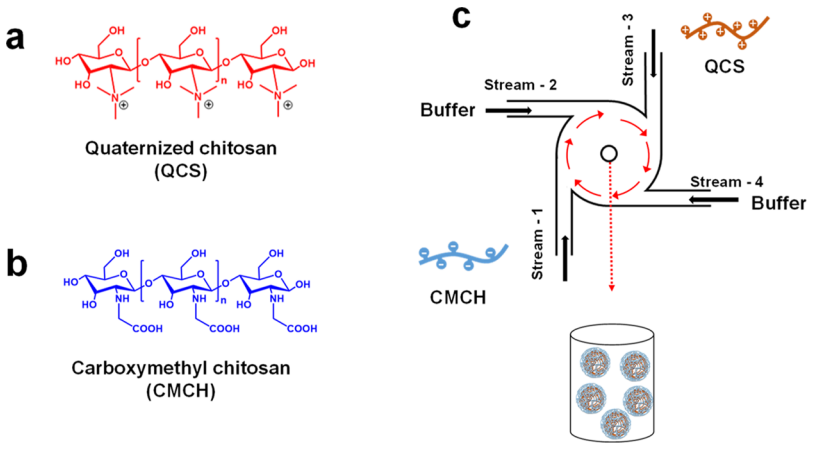

assembly at all production scales.[21,22] Great progress has been made in the past decade to obtain various kinds of NPs via FNP, such as drugs, imaging agents, genes, structured polymeric NPs, and so on.[23−32] Different from the common FNP method forming NPs based on solvent-induced supersaturation and precipitation of stabilizing polymers and hydrophobic active solutes, Zhu et al. first proposed in situ reactive flash nanoprecipitation (RFNP) and used RFNP to construct NPs through fast coupling two reactive end-capped polymers [PEG−NH_2 (methoxy−poly(ethylene glycol)−amine) and PCL−COCl (poly(ε-caprolactone)−acetyl chloride)].[16] Later, Zhu et al. further developed the RFNP method, in which water-soluble polyelectrolytes could be used instead of common-used amphiphilic block copolymer to prepare NPs such as linear or branched polyethyleneimine, chitosan, and ε-polylysine.[17] Thus, the RFNP method together with a polyelectrolyte stabilizer allows the possible reduced usage or even no organic solvent in the production of NPs.[17] Santos et al. prepared polyplex NPs of gene−polyethylenimine with polyionic pairing in the absence of any organic solvent, through in situ RFNP,[24] and Pinkerton et al. prepared organic active component NPs with ion pairing through in situ RFNP.[33] Meanwhile, Zhu et al. successfully acquired the time scales of the rapid mixing and the competing reactions during RFNP, which provided guidance to improve the desired coupling conversion of the reaction during RFNP.[34] More recently, Zhu et al. utilized in situ RFNP and realized fast generation and separation of NPs stabilized by a pH-sensitive polyelectrolyte without using any organic solvent, which was promising for large-scale industrial production.[35] In addition, nanoscale bioactive glass particles with doping of calcium were also successfully prepared by RFNP.[36]

Here, in this work, we employ RFNP to study the in situ interaction between two long-chain polyelectrolytes under fast mixing and the formation of the NC. Two oppositely charged polyelectrolyte chitosan derivatives are used: cationic derivative quaternized chitosan (QCS) and anionic derivative carboxymethyl chitosan (CMCH, with −COOH groups).[37,38] Chitosan is chosen due to the long chain and abundance in nature, which is the most abundant biopolymer after cellulose and nontoxic, renewable, antibacterial, biodegradable, and biocompatible.[29,39,40] It is, therefore, the "green polymer" *par excellence*.[41] The interaction of the positive and negative chitosan derivative and formation of the NC under RFNP are investigated, as shown in Scheme 1.

The resultant stable NCs are characterized systematically in terms of the charge molar ratio, pH, polymer concentration, and NaCl concentration. This method allows the continuous and tunable production of NCs and has the potential for fast clinical translation.

2. RESULTS AND DISCUSSION

2.1. Behavior of Polymers as a Function of pH. A polyelectrolyte complex is generally considered to be driven by entropy gain from small ions released and potential energy drop due to increased electrostatic attraction. Both depend on the charge density of the polymer.[42−44] Therefore, zeta potential presents the surface charge of the particles as a function of pH, which plays an important role.[45] Their zeta potential reflects the charge of polyelectrolytes; therefore, the zeta potential of polyelectrolytes is measured at different pH values to find the appropriate conditions for forming polyelectrolyte complexes. Figure 1 shows the effect of pH

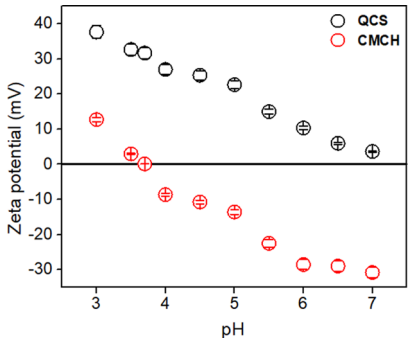

Figure 1. Zeta potential of QCS and CMCH in an aqueous solution at different pH values produced by acid/base titration. The concentration of QCS is 0.01 w/v %, and the concentration of CMCH is 0.02 w/v %.

on the zeta potential of QCS or CMCH in aqueous solutions. The CMCH molecules show cationic behavior at pH 3.0 and 3.5. CMCH has an isoelectric point (pI, at which the zeta potential reaches zero) at pH 3.7 due to its carboxyl groups. The zeta potential of CMCH becomes increasingly negative from approximately −8.63 to −30.7 mV as pH increases from 4.0 to 7.0. Meanwhile, QCS dispersion showed a positive charge value from pH 3.0 to 7.0 due to the quaternary ammonium groups. When the pH value reached 7.0, the

https://doi.org/10.1021/acsomega.1c02185
ACS Omega 2021, 6, 24526−24534

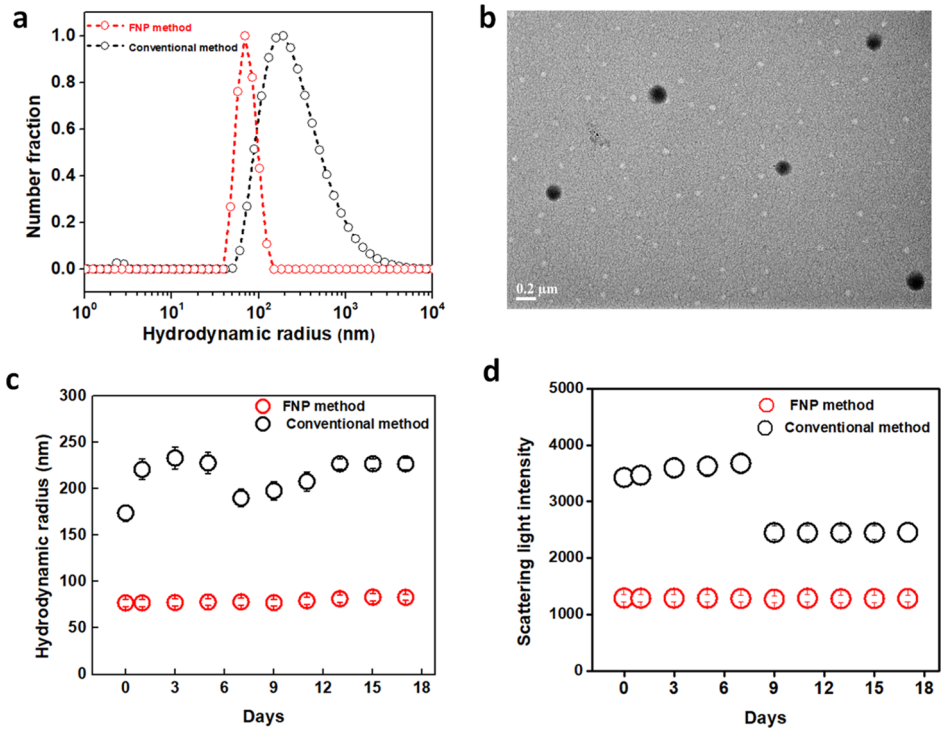

Figure 2. (a) NC size and size distribution prepared by RFNP (7 mL/min for each stream), comparing with the conventional self-assembly method; (b) TEM images of NCs designed by RFNP; (c) stability of NC size; and (d) scattering light intensity of NCs prepared by RFNP and conventional methods. The final concentration of the NC is 0.03 w/v %, QCS/CMCH = 1:2, and pH is 5.0.

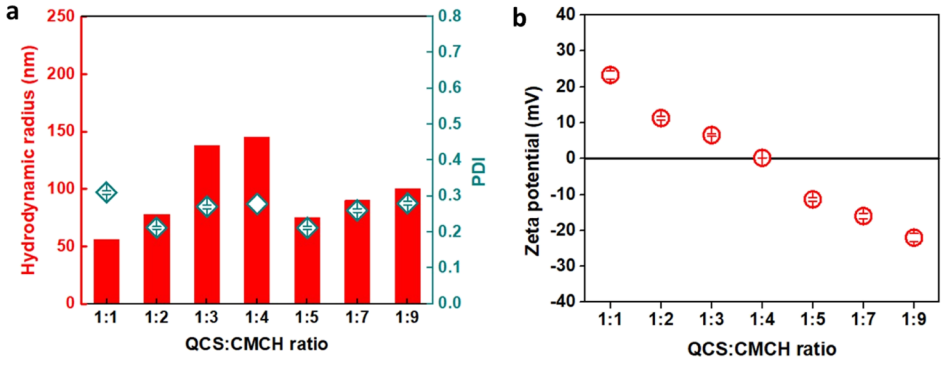

Figure 3. Effect of the charge molar ratio of QCS:CMCH on (a) hydrodynamics radius and PDI and (b) zeta potential at a fixed total polymer concentration (0.03 w/v %), pH 5.0, and flow rate of 7 mL/min.

positive charge decreased significantly. This phenomenon is usually attributed to the charge loss of the glucosamine fragment (pK_a 6.3−7.5),[40,46] and the decrease in the electrostatic shielding effect with the increase in NaOH addition neutralizes the pH value of the dispersion.

2.2. Comparison between RFNP and Self-Assembly Methods. NCs were prepared by RFNP through rapidly mixing polycation QCS and polyanion CMCH solutions at a flow rate of 7 mL/min and a concentration of 0.03 w/v %. The hydrodynamic radius measured by DLS is 77 nm (Figure 2a), and the size is evenly distributed, which is consistent with the TEM image (Figure 2b). Meanwhile, the obtained NCs by RFNP are very stable for over half a month, keeping a radius of around 79 nm (Figure 2c), polydispersity index (PDI) (Table S1), and constant scattering light intensity of around 1280 kHz (Table S1 and Figure 2d).

For comparison, the conventional self-assembled mixing method is also used to prepare NCs at the same polymer concentration. The obtained NCs have a higher radius of 178 nm with broader size distribution (Figure 2a). Simultaneously, the obtained NCs by the conventional method are not stable, experiencing a change in size and PDI, as shown in Figure 2c and Table S2, respectively. As shown in Figure 2d, there is a drop in light intensity on the ninth day due to the possible sedimentation of the aggregated large-size NC, indicating the instability of the NCs prepared by the conventional method.[17,26] Our results suggest that the RFNP method is more conducive to prepare small and stable NCs than the conventional method; meanwhile, it is demonstrated that nanoscale complexation occurs in different environments in these two processes.

The reproducibility and robustness of NC formation by the RFNP method are also confirmed. Different days are selected to produce three batches of NCs under the same conditions (final concentration of NC is 0.03 w/v %, QCS/CMCH = 1:2, and pH is 5.0). There is no significant variation in the size and

https://doi.org/10.1021/acsomega.1c02185
ACS Omega 2021, 6, 24526−24534

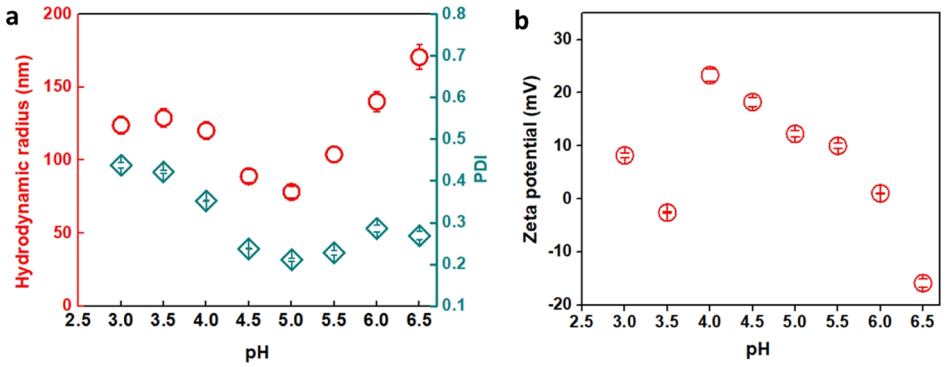

Figure 4. Effect of pH on (a) hydrodynamics radius and PDI and (b) zeta potential at a fixed total polymer concentration (0.03 w/v %), QCS/CMCH = 1:2, pH 5.0, and flow rate of 7 mL/min.

size distribution of NCs produced at different times, as shown in Table S3. The robustness and reproducibility of NCs are consistent with those previously described by Santos et al.[24] In the reported study, different operators produced three batches of NPs at different times to demonstrate the robustness and reproducibility of the NP formation in a confined impinging jet system. There was no significant batch-to-batch variability measured by DLS analysis.[24] This means that RFNP is an effective, scalable, and reproducible method that can operate in the continuous mode. Below, we evaluate the effects of various factors to control the NCs, such as the charge molar ratio, pH, flow rate, polymer concentration, and salt concentration.

2.3. Effect of the Charge Molar Ratio of QCS and CMCH. In order to control the formation and the surface charge of NCs, the key factor is the charge molar ratio of anionic to cationic polyelectrolytes during the complexation of CMCH and QCS in RFNP. Figure 3 shows the effect of different charge molar ratios of CMCH to QCS on the hydrodynamic radius and PDI of NCs. The sizes of the NCs are around 57, 78, 76, and 91 nm at 1:1, 1:3, 1:7, and 1:9, respectively, as shown in Figure 3a. It shows that the increase in CMCH leads to increasing NC sizes. Surprisingly, only the size of the polyelectrolyte complex at 1:3 ratio increased up to 138 ± 10 nm, and the PDI of 0.27 might be due to very low zeta potential (6.6 mV), as shown in Figure 3b. This can also be attributed to the charge switchover from positive to negative, accompanied by a sharp increase in the size of the polyelectrolyte complex. NCs are neutralized at a QCS/CMCH of about 1:4 and become negative when more CMCH is added at 1:5. It shows that CMCH molecules surround the QCS molecules. The gradual increase in the number of anionic polymers reduces the suspension's zeta potential to a negative value, indicating that QCS is completely neutralized. Similarly, increasing the amount of Kongda gum used to form the complex gradually reduced the zeta potential of the suspension to a negative value, indicating that chitosan was completely neutralized.[47] These results are consistent with those previously observed when the amount of chitosan was not enough to combine with the charge of pectin, leading to the system's negative characteristics due to the high concentration of pectin.[48]

With the further addition of CMCH, results in Figure 3 show that the current QCS is not enough to neutralize the CMCH, and CMCH containing COO^- in excess in chains becomes highly flexible, resulting in further negative characteristics of the system, forming anionic NCs from QCS/CMCH = 1:5−1:9. Meanwhile, the size distributions of NCs are in the same range (0.21−0.23). The lower size distribution would favor a complete ion pairing with QCS, leading to quasineutral complexes without enough unpaired carboxyl functions to stabilize particles. This increase in the negative surface charge is likely to form a negative coating around the QCS. The amount of CMCH per chitosan appears to play an essential role in the formation of NCs.

2.4. Effect of pH on the Polyelectrolyte Complexes of QCS and CMCH. Attractive interactions between oppositely charged polyelectrolytes can lead to a soluble or insoluble complex (phase separation/precipitation), and it depends on the polymer concentration, composition, and pH. The pH dependence of the size and the size distribution of NCs is shown in Figure 4. The results show that when the pH was reduced to 3.0, the size of NCs tended to be larger because both polyelectrolytes carried a similar net charge and repelled each other. Limited complexes are being formed, as confirmed by the lower scattering light intensities of the sample at pH 3.0 (Table S4). At pH 3.5, NCs show a higher size distribution (Figure 4a) due to the pI of CMCH (pI 3.7). There were no insoluble or precipitation (pHϕ1) complexes near the pI of CMCH (pH 3.5) due to the low polymer concentration. At pH 3.0, the NCs display a positive charge (12.7 mV), while the positive charge decreased to −2.6 mV at pH 3.5, which is expected to be weak complexation, as shown in Figure 4b. Above pH 4.0, biopolymers carry opposing net charges and begin to attract one another. Complexation is thought to occur as pH increases, large particles change into smaller particles, and the size distribution (Figure 4a) developed into a more homogeneous pattern than at lower pH values, suggesting the development of complexes between QCS and CMCH.

The development of complexes between QCS and CMCH can be observed by scattering light intensity. The polymer solution undergoes a transparent-to-cloudy transition, as evidenced by the significant increase in the scattering light intensity at which optimum interactions (pH_{opt}) between QCS and CMCH occur. These results demonstrate that the polymer mixture's pH-dependent increase in scattering intensity is due to the electrostatic interaction between QCS and CMCH. These results are consistent with those previously observed that the increase in the scattering light intensity with the pH value in the biopolymer mixture is due to the electrostatic interaction between whey proteins and gum arabic.[49] Similarly, the turbidity of particles slightly increased during complex formation.[50] With pH increasing from 5.0 to 6.5, the size and distribution of NCs increase as the positive charge decreased. This can be attributed to enhancing the deprotonation of

https://doi.org/10.1021/acsomega.1c02185
ACS Omega 2021, 6, 24526−24534

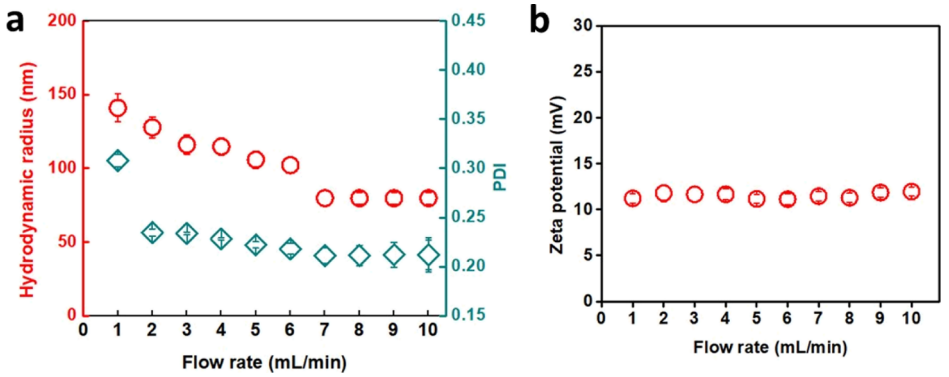

Figure 5. Effect of the flow rate on (a) hydrodynamics radius and PDI and (b) zeta potential at a fixed total polymer concentration (0.03 w/v %), QCS/CMCH = 1:2, and pH 5.0.

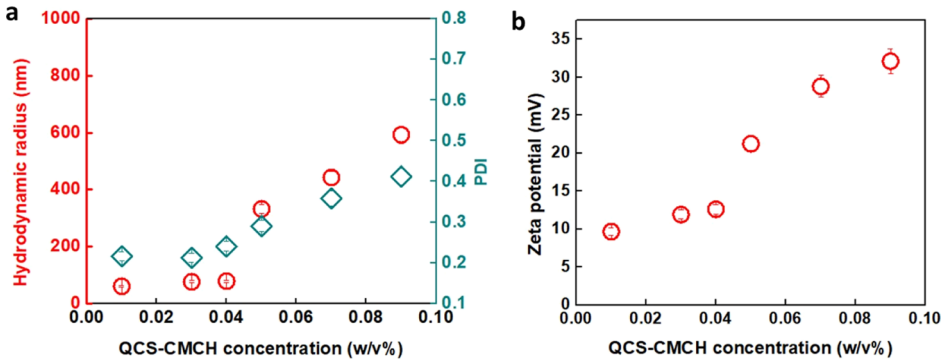

Figure 6. Effect of polymer concentration on (a) hydrodynamics radius and PDI and (b) zeta potential at a fixed flow rate of 7 mL/min, QCS/CMCH = 1:2, and pH 5.0.

amino groups in QCS (decrease in charge to the neutral value) and increasing the negative charge of COO^- groups on CMCH. Similarly, Yan et al.[10] also found that the zeta potential of the complex decreased with the rise in the pH value. The results demonstrate that the charge of the NCs is affected by pH. The lowest radius (74.8 nm) of NCs is found at pH 5.0 due to the maximum attraction of positive and negative molecules.

2.5. Effect of the Flow Rate on Complexation. The flow rate and the degree of mixing are the crucial characteristics of RFNP. Rapid mixing induces fast and homogeneous mixing of the polyanion and polycation.[27,51,52] We vary the flow rate from 1 mL/min to 10 mL/min [the corresponding Reynolds number (Re) shown in Table S5] for CMCH-QCS, at 0.03 w/v % and 1:2 ratio and maintaining the pH at 5.0. As shown in Figure 5a, as the flow rate increases from 1 mL/min to 7 mL/min, the radius decreases from 142 nm to around 74 nm, reaching the smallest size, and the size distribution is narrower from 0.31 to 0.24 (Figure 5a). When the flow rates are higher than 7 mL/min (Re ≈ 406), the size remains constant at around 76 nm, suggesting intensive mixing under these conditions.[25,26,51,52] These results are consistent with the literature results observed for amphiphilic polymer NPs prepared by the RFNP method, where the NP size becomes independent at a high flow rate at a fixed polymer concentration.[27]

The particle size and its distribution of the polyelectrolyte complex depend on the nature energy input. This may be because the high viscosity of polymer solution reduced the mixing efficiency or it did not have enough time to deform the particles. When the flow rate is high enough (i.e., 7 mL/min or Re ≈ 406), the mixing time is in the order of a few milliseconds, and the flow pattern assumes turbulent-like characteristics. Similarly, other types of mixing devices are used to achieve mixing regimes similar to RFNP. Liu et al., for example, reported a microfluidic glass capillary assembly that used a coaxial flow to achieve a homogeneous environment for NP nucleation and growth in Re ≈ 10−200 range.[53] The mixing time is a function of the flow rate. The mixing time (τ_{mix}) was not short enough to provide a homogeneous micromixing environment at a lower flow rate, resulting in the larger size and broad size distribution of NPs.[19,23,25,52,54] In a word, a higher flow rate enhances the mixing of the polyanion and polycation and shortens the mixing time, increasing the rate of energy dissipation, thus reducing the size of the particles and narrowing the size distribution. RFNP can prevent growth and aggregation faster, thus forming relatively stable NCs.[55,56] These results are consistent with those previously reported. According to Wang et al., RFNP NPs have a hydrodynamic radius of about 74 nm and narrow size distribution, while typical precipitation particles have larger sizes and a wider size spread.[26] We also demonstrated the effect of fast mixing on the polyelectrolyte complex NPs compared with self-assembly mixing. NCs keep a similar surface charge with speed changing from 1 to 10 mL/min, showing cationic NCs with 11.3 ± 1 mV at fixed 0.03 w/v % polymer concentration, as shown in Figure 5b.

2.6. Effect of Polymer Concentration. At a constant flow rate, that is, 7 mL/min (Re = 406), and charge molar ratio (QCS/CMCH = 1:2), with the increase in concentration from 0.03 to 0.09 w/v %, the radius of NCs significantly increases from 77 to 592 nm, while the size distribution increases from

https://doi.org/10.1021/acsomega.1c02185
ACS Omega 2021, 6, 24526−24534

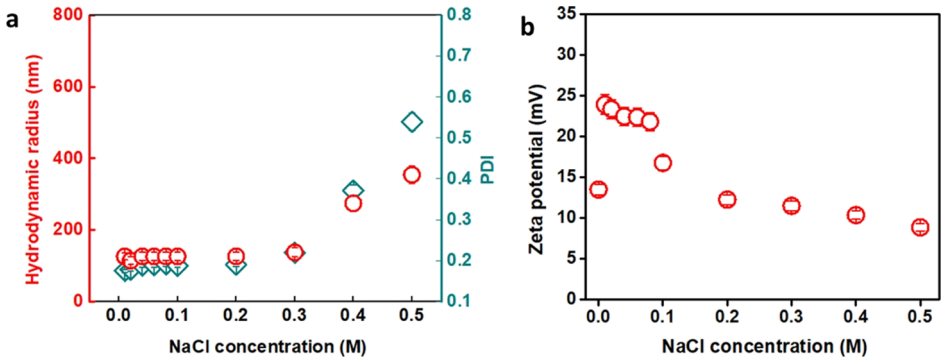

Figure 7. Effect of salt concentration on (a) hydrodynamics radius and PDI and (b) zeta potential at a fixed total polymer concentration (0.03 w/v %), QCS/CMCH = 1:2, QCS/CMCH = 1:2, pH 5.0, and flow rate of 7 mL/min.

0.21 to 0.36, as shown in Figure 6a. At higher concentrations above 0.03 w/v %, the size and size distribution increase. Beyond high concentrations of 0.1 w/v %, the prepared NC solution quickly precipitates. These results indicate that in the concentration range from 0.01 to 0.1 w/v %, the NC could be produced by RFNP. In comparison, the large-scale particle larger than 1 μm was formed through the conventional method by either QCS−CMCH or single chitosan derivatives (Figure S1).

Furthermore, the NCs exhibit an increased positive zeta potential (Figure 6b). The positive charge on NCs increased from +11.5 to +28.8 mV as concentration increased due to the loss of charge on CMCH. This may be attributed to the fact that the zeta potentials of the QCS solution were higher than those of the CMCH solution, yielding a cationic charge in the final mixture when the order of polymer is QCS:CMCH. Results indicated that when the polymer order was inversed (CMCH:QCS), NCs show larger size, and higher size distribution of cationic particles is obtained (Figure S2).

2.7. Effect of Salt on Complexation. As the NCs are charged, consisting of electrostatically driven complexes, the electrostatic interaction and the formation of NCs could be affected by ionic strength or salt concentration. As shown in Figure 7a, the radius of NC is around 77 nm in the absence of NaCl. With the addition of NaCl, the size increased to 106 nm, and with the further increase in NaCl concentration to 0.3 M, the radius increased slightly from 106.5 to 136 nm with uniform size distribution (from 0.14 to 0.20). After that, ionic strength significantly affects NC complexation. Remarkably, the hydrodynamic radius of the NC increased from 309 to 502 nm, and higher PDI (0.34 and 0.41) values are obtained, respectively, at 0.4 and 0.5 M (Figure 7a). The significant increase in the radius of the NC at 0.4 and 0.5 M suggests that the aggregation and successive sedimentation of particles are indeed observed after overnight storage. In general, high salt concentrations have a dissociating effect on coacervate complexes.[57] We assume that the increase in the size of NCs with the increase in NaCl concentration reflects the influence on the formation of the QCS−CMCH complex in two ways: (1) screening the electrostatic repulsion between the aggregation subunits, which increases the collision frequency, and (2) the competitive binding of CMCH anions and Cl^-, weakening the binding of QCS−CMCH. Although the weakened QCS−CMCH binding slows down the formation and aggregation of NCs (both need to be linked to the chitosan chain via CMCH), which was again consistent with previous work. The zeta potential increased from 13.5 mV for the NC without salt to 23.7 mV for the NC with 0.01M salt and around 22 mV with 0.01−0.08M salt. This indicates the attraction between polymers and the addition of a small amount of NaCl, which enhances the polyelectrolyte complex by increasing the solubility of the polymers and is favorable to the electrostatic attraction up to 0.08 M.[50]

However, no macroscopic phase separation occurred. Besides, the zeta potential decreased from 21.8 to 8.8 mV as NaCl concentration increased from 0.1 to 0.5 M. The increase in NaCl concentration weakens electrostatic interactions (electrostatic screening effects) between oppositely charged polymers, resulting in complex destruction between QCS and CMCH. In general, the conductivity of the solution increases with the increase in the salt content (Table S6).

3. CONCLUSIONS

We successfully prepared nanoscale polyelectrolyte complexes with uniform size by RFNP using QCS as a polycation and CMCH as a polyanion. The size of NCs can be modulated by altering the volumetric flow rates of streams. The prepared NCs depend on the pH, the concentration, and the cationic/anionic ratio of biopolymers. The charge molar ratio of the polyanion to the polycation was also tuned to create NCs with a positive or negative shell. Meanwhile, the NPs prepared have no significant batch-to-batch variability, which will be beneficial to the continuous and reproducible production of nanoscale polyelectrolyte complexes. These results indicate that the nanoscale polyelectrolyte complex could be effectively prepared by RFNP and will be helpful in many applications, such as drug delivery and food processing.

4. MATERIALS AND METHODS

4.1. Materials. QCS (M_w = 200 kDa, degree of substitution >80%) and CMCH (M_w = 200 kDa, degree of substitution >90%) were purchased from Nantong Lushen Bioengineering Co.; sodium chloride (NaCl), hydrochloric acid (HCl), sodium hydroxide (NaOH), and acetic acid were purchased from Sigma-Aldrich (Shanghai, China). Milli-Q water was used for the preparation of all solutions.

4.2. Solution Preparation. QCS stock solutions were prepared by dissolving the dry powder in acetic acid (83.3 mM) and stirring at room temperature overnight. CMCH stock solutions were prepared by dispersing the powder into sodium acetate buffer (5 mM, pH 7.0) and subsequently stirring for at least 4 h to ensure complete dissolution. The pH of QCS, CMCH, or QCS/CMCH was adjusted using 1.0, 0.5, and 0.1 M NaOH or HCl as needed. The effect of ionic

https://doi.org/10.1021/acsomega.1c02185
ACS Omega 2021, 6, 24526−24534

strength is investigated at different NaCl (0−0.5 M) concentrations before mixing in a separate syringe.

4.3. Preparation of NCs. The multi-inlet vortex mixer device consists of four inlets, as shown in Scheme 1 (c). Streams 2 and 4 were arranged for the buffer of the same pH as a polymer solution, stream 1 was arranged for the CMCH solution, and stream 3 was arranged for the QCS solution. To investigate the effect of ionic strength, stream 2 was used to inject an aqueous solution of NaCl with the same pH through inlets 1, 3, and 4. Various concentrations of QCS and CMCH were investigated to optimize the NCs. The four streams were all connected to the syringe via Teflon tubing. The volumetric flow rates for the four streams were the same (1−10 mL/min).

4.4. Characterization of NCs. For zeta potential values, a Zetasizer instrument (Malvern Instruments, ZEN 3700, Zeta master, Worcs., UK) measured the charge on particles at room temperature. Equipment software uses the Smoluchowski mathematical model to convert the electrophoretic mobility measurement value into the zeta potential value.

For NC sizes, the mean hydrodynamic radius (R_h) was measured by dynamic−static light scattering (ALV-CGS3 light scattering apparatus, operating at a wavelength of 632.8 nm) at 25 °C. R_h is measured at a fixed angle of 90°. The CONTIN method was used to analyze the size distribution of particles. Scattering light intensity is also recorded while measuring the size of NCs. For data processing, average and standard deviations were obtained from six duplicates with acquisition times of 30 s for each.

For morphology, NC morphology was observed by TEM (TEM, Hitachi, H-700 Tokyo, Japan). A drop of NCs of the solution was deposited on a carbon-coated copper grid. The droplet was allowed to dry for 10 min.

■ ASSOCIATED CONTENT

Supporting Information

The Supporting Information is available free of charge at https://pubs.acs.org/doi/10.1021/acsomega.1c02185.

Light scattering intensity of NCs prepared by RFNP, particle size distribution of NCs prepared by the conventional method, reproducibility of NCs by RFNP, scattering light intensity of NCs at different pH values, calculated Re number of each run for different NCs, effect of polymer concentration on the hydrodynamics radius and PDI of the complex formed by QCS and CMCH by the conventional method and the particle formed by only QCS and CMCH at pH 5.0, effect of the weight ratio and order of polymer addition, CMCH:QCS, on the hydrodynamic radius and zeta potential of NCs, and salt concentration effect on the conductivity and light scattering intensity of NCs (PDF)

■ AUTHOR INFORMATION

Corresponding Authors

Mingwei Wang − *State-Key Laboratory of Chemical Engineering, and Shanghai Key Laboratory of Multiphase Materials Chemical Engineering, East China University of Science and Technology, Shanghai 200237, People's Republic of China;* orcid.org/0000-0001-7071-9166; Email: mingweiwang@ecust.edu.cn

Xuhong Guo − *State-Key Laboratory of Chemical Engineering, and Shanghai Key Laboratory of Multiphase Materials Chemical Engineering, East China University of Science and Technology, Shanghai 200237, People's Republic of China; International Joint Research Center of Green Energy Chemical Engineering, East China University of Science and Technology, Shanghai 200237, P.R. China; Engineering Research Center of Materials Chemical Engineering of Xinjiang Bingtuan, Shihezi University, Shihezi, Xinjiang 832000, P.R. China;* orcid.org/0000-0002-1792-8564; Email: guoxuhong@ecust.edu.cn

Authors

Rizwan Ahmed − *State-Key Laboratory of Chemical Engineering, and Shanghai Key Laboratory of Multiphase Materials Chemical Engineering, East China University of Science and Technology, Shanghai 200237, People's Republic of China*

Noor ul ain Hira − *State Key Laboratory of Advanced Polymeric Material, School of Materials Science and Engineering, East China University of Science and Technology, Shanghai 200237, P.R. China*

Zhinan Fu − *State-Key Laboratory of Chemical Engineering, and Shanghai Key Laboratory of Multiphase Materials Chemical Engineering, East China University of Science and Technology, Shanghai 200237, People's Republic of China*

Adeel Halepoto − *State-Key Laboratory of Chemical Engineering, and Shanghai Key Laboratory of Multiphase Materials Chemical Engineering, East China University of Science and Technology, Shanghai 200237, People's Republic of China*

Santosh Khanal − *State Key Laboratory of Advanced Polymeric Material, School of Materials Science and Engineering, East China University of Science and Technology, Shanghai 200237, P.R. China*

Shahid Iqbal − *School of Chemical and Environmental Engineering, College of Chemistry, Chemical Engineering and Materials Science, Soochow University, Suzhou, Jiangsu 215123, China*

Hidayatullah Mahar − *National Fertilizer Corporation (NFC) Institute of Engineering & Technology, Chemical Engineering, Multan 60000, Pakistan*

Martien Abraham Cohen Stuart − *State-Key Laboratory of Chemical Engineering, and Shanghai Key Laboratory of Multiphase Materials Chemical Engineering, East China University of Science and Technology, Shanghai 200237, People's Republic of China;* orcid.org/0000-0001-6880-7861

Complete contact information is available at: https://pubs.acs.org/10.1021/acsomega.1c02185

Author Contributions

¶R.A. and N.u.a.H. contributed equally.

Notes

The authors declare no competing financial interest.

■ ACKNOWLEDGMENTS

This work was supported by the National Natural Science Foundation of China (NSFC) for Young Scholars (21706074), "1000 Foreign Experts Program" (WQ20163100341).

■ REFERENCES

(1) Sanna, V.; Sechi, M. Therapeutic Potential of Targeted Nanoparticles and Perspective on Nanotherapies. *ACS Med. Chem. Lett.* **2020**, *11*, 1069−1073.

(2) Kumar, R.; Dalvi, S. V.; Siril, P. F. Nanoparticle-Based Drugs and Formulations: Current Status and Emerging Applications. *ACS Appl. Nano Mater.* **2020**, *3*, 4944−4961.
(3) Salunkhe, A.; Khot, V.; Patil, S. I.; Tofail, S. A. M.; Bauer, J.; Thorat, N. D. MRI Guided Magneto-chemotherapy with High-Magnetic-Moment Iron Oxide Nanoparticles for Cancer Theranostics. *ACS Appl. Bio Mater.* **2020**, *3*, 2305−2313.
(4) Hayashi, K.; Sato, Y.; Sakamoto, W.; Yogo, T. Theranostic Nanoparticles for MRI-Guided Thermochemotherapy: "Tight" Clustering of Magnetic Nanoparticles Boosts Relaxivity and Heat-Generation Power. *ACS Biomater. Sci. Eng.* **2017**, *3*, 95−105.
(5) Kulkarni, A. D.; Vanjari, Y. H.; Sancheti, K. H.; Patel, H. M.; Belgamwar, V. S.; Surana, S. J.; Pardeshi, C. V. Polyelectrolyte complexes: mechanisms, critical experimental aspects, and applications. *Artif. Cells, Nanomed., Biotechnol.* **2016**, *44*, 1615−1625.
(6) Kim, S.; Sureka, H. V.; Kayitmazer, A. B.; Wang, G.; Swan, J. W.; Olsen, B. D. Effect of Protein Surface Charge Distribution on Protein-Polyelectrolyte Complexation. *Biomacromolecules* **2020**, *21*, 3026−3037.
(7) Wang, F.; Yang, Y.; Ju, X.; Udenigwe, C. C.; He, R. Polyelectrolyte Complex Nanoparticles from Chitosan and Acylated Rapeseed Cruciferin Protein for Curcumin Delivery. *J. Agric. Food Chem.* **2018**, *66*, 2685−2693.
(8) Sarika, P. R.; James, N. R. Polyelectrolyte complex nanoparticles from cationised gelatin and sodium alginate for curcumin delivery. *Carbohydr. Polym.* **2016**, *148*, 354−361.
(9) Lin, Y.-H.; Sonaje, K.; Lin, K. M.; Juang, J.-H.; Mi, F.-L.; Yang, H.-W.; Sung, H.-W. Multi-ion-crosslinked nanoparticles with pH-responsive characteristics for oral delivery of protein drugs. *J. Controlled Release* **2008**, *132*, 141−149.
(10) Yan, J.-K.; Qiu, W.-Y.; Wang, Y.-Y.; Wu, J.-Y. Biocompatible Polyelectrolyte Complex Nanoparticles from Lactoferrin and Pectin as Potential Vehicles for Antioxidative Curcumin. *J. Agric. Food Chem.* **2017**, *65*, 5720−5730.
(11) Machmudah, S.; Winardi, S.; Wahyudiono; Kanda, H.; Goto, M. Formation of Fine Particles from Curcumin/PVP by the Supercritical Antisolvent Process with a Coaxial Nozzle. *ACS Omega* **2020**, *5*, 6705−6714.
(12) Liu, Z.; Jiao, Y.; Wang, Y.; Zhou, C.; Zhang, Z. Polysaccharides-based nanoparticles as drug delivery systems. *Adv. Drug Delivery Rev.* **2008**, *60*, 1650−1662.
(13) Johnson, B. K.; Prud'homme, R. K. Flash NanoPrecipitation of Organic Actives and Block Copolymers using a Confined Impinging Jets Mixer. *Aust. J. Chem.* **2003**, *56*, 1021.
(14) Johnson, B. K.; Prud'homme, R. K. Mechanism for Rapid Self-Assembly of Block Copolymer Nanoparticles. *Phys. Rev. Lett.* **2003**, *91*, 118302.
(15) Johnson, B. K.; Prud'homme, R. K. Chemical processing and micromixing in confined impinging jets. *AIChE J.* **2004**, *49*, 2264−2282.
(16) Zhu, Z.; Anacker, J. L.; Ji, S.; Hoye, T. R.; Macosko, C. W.; Prud'homme, R. K. Formation of block copolymer-protected nanoparticles via reactive impingement mixing. *Langmuir* **2007**, *23*, 10499−10504.
(17) Zhu, Z.; Margulis-Goshen, K.; Magdassi, S.; Talmon, Y.; Macosko, C. W. Polyelectrolyte Stabilized Drug Nanoparticles via Flash Nanoprecipitation: A Model Study With β-Carotene. *J. Pharm. Sci.* **2010**, *99*, 4295−4306.
(18) Han, J.; Zhu, Z.; Qian, H.; Wohl, A. R.; Beaman, C. J.; Hoye, T. R.; Macosko, C. W. A simple confined impingement jets mixer for flash nanoprecipitation. *J. Pharm. Sci.* **2012**, *101*, 4018−4023.
(19) Zhu, Z. Effects of amphiphilic diblock copolymer on drug nanoparticle formation and stability. *Biomaterials* **2013**, *34*, 10238−10248.
(20) Zhu, Z. Flash nanoprecipitation: prediction and enhancement of particle stability via drug structure. *Mol. Pharm.* **2014**, *11*, 776−786.
(21) Liu, Y.; Kathan, K.; Saad, W.; Prud'homme, R. K. Ostwald ripening of beta-carotene nanoparticles. *Phys. Rev. Lett.* **2007**, *98*, 036102.
(22) D'Addio, S. M.; Prud'homme, R. K. Controlling drug nanoparticle formation by rapid precipitation. *Adv. Drug Delivery Rev.* **2011**, *63*, 417−426.
(23) Wang, M.; Yang, N.; Guo, Z.; Gu, K.; Shao, A.; Zhu, W.; Xu, Y.; Wang, J.; Prud'homme, R. K.; Guo, X. Facile Preparation of AIE-Active Fluorescent Nanoparticles through Flash Nanoprecipitation. *Ind. Eng. Chem. Res.* **2015**, *54*, 4683−4688.
(24) Santos, J. L.; Ren, Y.; Vandermark, J.; Archang, M. M.; Williford, J.-M.; Liu, H.-W.; Lee, J.; Wang, T.-H.; Mao, H.-Q. Continuous Production of Discrete Plasmid DNA-Polycation Nanoparticles Using Flash Nanocomplexation. *Small* **2016**, *12*, 6214−6222.
(25) Wang, M.; Xu, Y.; Liu, Y.; Gu, K.; Tan, J.; Shi, P.; Yang, D.; Guo, Z.; Zhu, W.; Guo, X.; Cohen Stuart, M. A. Morphology Tuning of Aggregation-Induced Emission Probes by Flash Nanoprecipitation: Shape and Size Effects on in Vivo Imaging. *ACS Appl. Mater. Interfaces* **2018**, *10*, 25186−25193.
(26) Wang, M.; Lin, S.; Wang, J.; Liu, L.; Zhou, W.; Ahmed, R. B.; Hu, A.; Guo, X.; Cohen Stuart, M. A. Controlling Morphology and Release Behavior of Sorafenib-Loaded Nanocarriers Prepared by Flash Nanoprecipitation. *Ind. Eng. Chem. Res.* **2018**, *57*, 11911−11919.
(27) He, Z.; Santos, J. L.; Tian, H.; Huang, H.; Hu, Y.; Liu, L.; Leong, K. W.; Chen, Y.; Mao, H.-Q. Scalable fabrication of size-controlled chitosan nanoparticles for oral delivery of insulin. *Biomaterials* **2017**, *130*, 28−41.
(28) He, Z.; Liu, Z.; Tian, H.; Hu, Y.; Liu, L.; Leong, K. W.; Mao, H.-Q.; Chen, Y. Scalable production of core-shell nanoparticles by flash nanocomplexation to enhance mucosal transport for oral delivery of insulin. *Nanoscale* **2018**, *10*, 3307−3319.
(29) Yuan, Y.; Huang, Y. Ionically crosslinked polyelectrolyte nanoparticle formation mechanisms: the significance of mixing. *Soft Matter* **2019**, *15*, 9871−9880.
(30) Akbulut, M.; Ginart, P.; Gindy, M. E.; Theriault, C.; Chin, K. H.; Soboyejo, W.; Prud'homme, R. K. Generic Method of Preparing Multifunctional Fluorescent Nanoparticles Using Flash NanoPrecipitation. *Adv. Funct. Mater.* **2009**, *19*, 718−725.
(31) Grundy, L. S.; Lee, V. E.; Li, N.; Sosa, C.; Mulhearn, W. D.; Liu, R.; Register, R. A.; Nikoubashman, A.; Prud'homme, R. K.; Panagiotopoulos, A. Z.; Priestley, R. D. Rapid Production of Internally Structured Colloids by Flash Nanoprecipitation of Block Copolymer Blends. *ACS Nano* **2018**, *12*, 4660−4668.
(32) Kumar, V.; Hong, S. Y.; Maciag, A. E.; Saavedra, J. E.; Adamson, D. H.; Prud'homme, R. K.; Keefer, L. K.; Chakrapani, H. Stabilization of the nitric oxide (NO) prodrugs and anticancer leads, PABA/NO and Double JS-K, through incorporation into PEG-protected nanoparticles. *Mol. Pharm.* **2010**, *7*, 291−298.
(33) Pinkerton, N. M.; Grandeury, A.; Fisch, A.; Brozio, J.; Riebesehl, B. U.; Prud'homme, R. K. Formation of stable nanocarriers by in situ ion pairing during block-copolymer-directed rapid precipitation. *Mol. Pharm.* **2013**, *10*, 319−328.
(34) Zhu, Z.; Wang, X. Simulations on time scales and conversion of fast competing reactions in rapid mixing. *Chem. Eng. J.* **2018**, *336*, 741−747.
(35) Zhu, Z.; Xu, P.; Fan, G.; Liu, N.; Xu, S.; Li, X.; Xue, H.; Shao, C.; Guo, Y. Fast synthesis and separation of nanoparticles via in-situ reactive flash nanoprecipitation and pH tuning. *Chem. Eng. J.* **2019**, *356*, 877−885.
(36) Ji, L.; Xu, T.; Gu, J.; Liu, Q.; Zhou, S.; Shi, G.; Zhu, Z. Preparation of bioactive glass nanoparticles with highly and evenly doped calcium ions by reactive flash nanoprecipitation. *J. Mater. Sci.: Mater. Med.* **2021**, *32*, 48.
(37) Kalliola, S.; Repo, E.; Srivastava, V.; Heiskanen, J. P.; Sirviö, J. A.; Liimatainen, H.; Sillanpää, M. The pH sensitive properties of carboxymethyl chitosan nanoparticles cross-linked with calcium ions. *Colloids Surf., B* **2017**, *153*, 229−236.
(38) Kalliola, S.; Repo, E.; Srivastava, V.; Zhao, F.; Heiskanen, J. P.; Sirviö, J. A.; Liimatainen, H.; Sillanpää, M. Carboxymethyl Chitosan

https://doi.org/10.1021/acsomega.1c02185
ACS Omega 2021, 6, 24526−24534

and Its Hydrophobically Modified Derivative as pH-Switchable Emulsifiers. *Langmuir* **2018**, *34*, 2800−2806.
(39) Meka, V. S.; Sing, M. K. G.; Pichika, M. R.; Nali, S. R.; Kolapalli, V. R. M.; Kesharwani, P. A comprehensive review on polyelectrolyte complexes. *Drug Discovery Today* **2017**, *22*, 1697−1706.
(40) Bhutto, R. A.; Wang, M.; Qi, Z.; Hira, N. u. a.; Jiang, J.; Zhang, H.; Iqbal, S.; Wang, J.; Stuart, M. A. C.; Guo, X. Pickering Emulsions Based on the pH-Responsive Assembly of Food-Grade Chitosan. *ACS Omega* **2021**, *6*, 17915.
(41) Gierszewska, M.; Ostrowska-Czubenko, J.; Chrzanowska, E. pH-responsive chitosan/alginate polyelectrolyte complex membranes reinforced by tripolyphosphate. *Eur. Polym. J.* **2018**, *101*, 282−290.
(42) Kayitmazer, A. B.; Bohidar, H. B.; Mattison, K. W.; Bose, A.; Sarkar, J.; Hashidzume, A.; Russo, P. S.; Jaeger, W.; Dubin, P. L. Mesophase separation and probe dynamics in protein-polyelectrolyte coacervates. *Soft Matter* **2007**, *3*, 1064−1076.
(43) Hofs, B.; de Keizer, A.; van der Burgh, S.; Leermakers, F. A. M.; Cohen Stuart, M. A.; Millard, P.-E.; Müller, A. H. E. Complex coacervate core micro-emulsions. *Soft Matter* **2008**, *4*, 1473−1482.
(44) Brzozowska, A. M.; Spruijt, E.; de Keizer, A.; Cohen Stuart, M. A.; Norde, W. On the stability of the polymer brushes formed by adsorption of ionomer complexes on hydrophilic and hydrophobic surfaces. *J. Colloid Interface Sci.* **2011**, *353*, 380−391.
(45) Schmitt, C.; Turgeon, S. L. Protein/polysaccharide complexes and coacervates in food systems. *Adv. Colloid Interface Sci.* **2011**, *167*, 63−70.
(46) Wang, X.-Y.; Heuzey, M.-C. Chitosan-Based Conventional and Pickering Emulsions with Long-Term Stability. *Langmuir* **2016**, *32*, 929−936.
(47) Naidu, V. G. M.; Madhusudhana, K.; Sashidhar, R. B.; Ramakrishna, S.; Khar, R. K.; Ahmed, F. J.; Diwan, P. V. Polyelectrolyte complexes of gum kondagogu and chitosan, as diclofenac carriers. *Carbohydr. Polym.* **2009**, *76*, 464−471.
(48) Maciel, V. B. V.; Yoshida, C. M. P.; Franco, T. T. Chitosan/pectin polyelectrolyte complex as a pH indicator. *Carbohydr. Polym.* **2015**, *132*, 537−545.
(49) Weinbreck, F.; de Vries, R.; Schrooyen, P.; de Kruif, C. G. Complex Coacervation of Whey Proteins and Gum Arabic. *Biomacromolecules* **2003**, *4*, 293−303.
(50) Xiong, W.; Ren, C.; Jin, W.; Tian, J.; Wang, Y.; Shah, B. R.; Li, J.; Li, B. Ovalbumin-chitosan complex coacervation: Phase behavior, thermodynamic and rheological properties. *Food Hydrocolloids* **2016**, *61*, 895−902.
(51) Fu, Z.; Li, L.; Li, F.; Bhutto, R. A.; Niu, X.; Liu, D.; Guo, X. Facile Morphology Control during Rapid Fabrication of Nanosized Organosilica Particles. *Ind. Eng. Chem. Res.* **2020**, *59*, 14797−14805.
(52) Yu, J.; Wang, M.; Bhutto, R. A.; Zhao, H.; Cohen Stuart, M. A.; Wang, J. Facile Preparation of Tilmicosin-Loaded Polymeric Nanoparticle with Controlled Properties and Functions. *ACS Omega* **2020**, *5*, 32366−32372.
(53) Liu, D.; Cito, S.; Zhang, Y.; Wang, C.-F.; Sikanen, T. M.; Santos, H. A. A Versatile and Robust Microfluidic Platform Toward High Throughput Synthesis of Homogeneous Nanoparticles with Tunable Properties. *Adv. Mater.* **2015**, *27*, 2298−2304.
(54) Ahmed Bhutto, R.; Fu, Z.; Wang, M.; Yu, J.; Zhao, F.; Khanal, S.; Halepoto, A.; Wang, J.; Cohen Stuart, M. A.; Guo, X. Facile controlling internal structure of β-carotene-loaded protein nanoparticles by Flash Nanoprecipitation. *Mater. Lett.* **2021**, *304*, 130523.
(55) Liu, Y.; Cheng, C.; Liu, Y.; Prud'homme, R. K.; Fox, R. O. Mixing in a multi-inlet vortex mixer (MIVM) for flash nanoprecipitation. *Chem. Eng. Sci.* **2008**, *63*, 2829−2842.
(56) Tu, T.; Zhou, W.; Wang, M.; Guo, X.; Li, L.; Cohen Stuart, M. A.; Wang, J. One-Pot Synthesis of Small and Uniform Gold Nanoparticles in Water by Flash Nanoprecipitation. *Ind. Eng. Chem. Res.* **2020**, *59*, 11080−11086.
(57) Moschakis, T.; Biliaderis, C. G. Biopolymer-based coacervates: Structures, functionality and applications in food products. *Curr. Opin. Colloid Interface Sci.* **2017**, *28*, 96−109.

https://doi.org/10.1021/acsomega.1c02185
ACS Omega 2021, 6, 24526−24534